Published in final edited form as:
Limnol Oceanogr. 2010 March ; 55(2): 703–713.

Contribution of mycosporine-like amino acids and colored dissolved and particulate matter to sea ice optical properties and ultraviolet attenuation

Jari Uusikivi[a,*], **Anssi V. Vähätalo**[b], **Mats A. Granskog**[c,d], and **Ruben Sommaruga**[e]

[a]Department of Physics, University of Helsinki, Helsinki, Finland [b]Department of Biological and Environmental Sciences, University of Helsinki, Helsinki, Finland [c]Arctic Centre, Rovaniemi, Finland [d]Norwegian Polar Institute, The Polar Environmental Centre, Tromsø, Norway [e]Laboratory of Aquatic Photobiology and Plankton Ecology, Institute of Ecology, University of Innsbruck, Innsbruck, Austria

Abstract

In the Baltic Sea ice, the spectral absorption coefficients for particulate matter (PM) were about two times higher at ultraviolet wavelengths than at photosynthetically available radiation (PAR) wavelengths. PM absorption spectra included significant absorption by mycosporine-like amino acids (MAAs) between 320 and 345 nm. In the surface ice layer, the concentration of MAAs (1.37 μg L^{-1}) was similar to that of chlorophyll *a*, resulting in a MAAs-to-chlorophyll *a* ratio as high as 0.65. Ultraviolet radiation (UVR) intensity and the ratio of UVR to PAR had a strong relationship with MAAs concentration (R^2 = 0.97, n = 3) in the ice. In the surface ice layer, PM and especially MAAs dominated the absorption (absorption coefficient at 325 nm: 0.73 m^{-1}). In the columnar ice layers, colored dissolved organic matter was the most significant absorber in the UVR (< 380 nm) (absorption coefficient at 325 nm: 1.5 m^{-1}). Our measurements and modeling of UVR and PAR in Baltic Sea ice show that organic matter, both particulate and dissolved, influences the optical properties of sea ice and strongly modifies the UVR exposure of biological communities in and under snow-free sea ice.

The transmittance of solar radiation through ice is an important factor affecting biological activity in and under sea ice (Perovich et al. 1993; Perovich 2003). The most important factors controlling the transmission of light through a sea ice cover are the ice itself, gas and brine inclusions, particulate matter (PM), and colored (also called chromophoric) dissolved organic matter (CDOM) incorporated into the ice cover (Perovich et al. 1998; Belzile et al. 2000). Those materials are incorporated into the sea ice during its initial formation from parent seawater or originate from atmospheric deposition. However, both PM (algae) and CDOM produced in ice are also important for the optics of sea ice (Arrigo 2003; Thomas and Papadimitriou 2003). Gas inclusions (e.g., air bubbles) are typically concentrated to the surface scattering layer and are incorporated to the ice cover through snow ice formation or melting and refreezing of ice surface.

Photosynthetically active radiation (PAR, 400 to 700 nm) drives photosynthesis, whereas ultraviolet radiation (UVR, 280 to 400 nm) has many direct and indirect harmful effects on biota. Therefore, it is equally important to understand the penetration of both PAR and UVR

* Corresponding author: jari.uusikivi@helsinki.fi.

Europe PMC Funders Author Manuscripts

through the ice (Perovich 1993). The UVR attenuation properties of sea ice and the contribution of CDOM and PM to sea ice optical properties are little understood (Belzile et al. 2000). This is particularly important because earlier studies indicate that ice algae adapted to the low light conditions prevailing under snow and ice covers are potentially sensitive to UVR (Cota et al. 1991; Prezelin et al. 1998). In this context, CDOM can be both a shield from harmful UVR and a potential precursor for biologically labile compounds that could enhance biological activity; however, the overall effect to sea ice communities is not well known.

Another poorly known aspect of sea ice optical properties is the role of mycosporine-like amino acids (MAAs) for the attenuation of UVR in the sea ice cover. MAAs are a family of photoprotective compounds that have high molar extinction coefficients and therefore absorb UVR efficiently. Primary producers synthesize MAAs, which can attenuate UVR in the water column (Sommaruga and Psenner 1997; Laurion et al. 2000). Belzile et al. (2000) suggested the presence of MAAs in first-year ice in an Arctic polynya, but did not study them. Ryan et al. (2002) studied an Antarctic bottom-ice algal community and reported very low MAA concentrations and concluded that MAAs play a minor role in attenuation of UVR at the bottom of sea ice covers.

In this paper, we extend the analysis of sea ice optical properties from PAR to the UV range and address the contribution of CDOM and PM to the overall optical properties and quality of the light field within the ice. Special emphasis was given to the interaction between CDOM and biology with ice optical properties. This was accomplished by measurements of the spectral albedo, spectral light attenuation and transmittance of landfast sea ice, and the CDOM, PM, and MAAs absorption from melted ice samples. These results were then incorporated to a radiative transfer model to examine the role of CDOM and PM absorption to the overall optical properties of the sea ice cover in a range of conditions.

Methods

Study site

The study site was located at the entrance of the Gulf of Finland, Baltic Sea, near the Finnish coast. On the Finnish coast, landfast sea ice is generally formed every winter and lasts for 2 to 6 months. Although the salinity of the Baltic Sea surface water along the Finnish coast is normally between 2 and 6, the ice cover typically shows sea ice-like features, such as brine pockets and irregular crystal boundaries (Kawamura et al. 2001). At water salinities higher than about 0.6, the ice formed has sea ice characteristics, and therefore it is only in the proximity of river estuaries that Baltic Sea ice is directly comparable with freshwater ice (Palosuo 1961). Granular surface ice layers, composed of snow ice and superimposed ice, usually contribute up to half of total landfast ice thickness in the Baltic Sea (Kawamura et al. 2001; Granskog et al. 2004). These highly scattering surface layers affect significantly the overall optical properties of the relatively thin Baltic Sea ice cover (Ehn et al. 2004).

Fieldwork was conducted from 13 to 15 March 2007 on landfast sea ice at Santala Bay (59°55′N, 23°05′E). Santala Bay is a semienclosed bay sheltered from open sea by a peninsula and islands, thereby allowing fast ice to form even in mild winters (Granskog et al. 2004). Winter 2007 was mild and at time of measurements, the ice cover was about 2 months old and 37 cm thick. On the basis of structural analyses, the ice cover consisted of 31-cm columnar ice and a 6-cm granular ice layer at the surface. Ice cover thickness and structure were typical for the area during mild winters (Granskog et al. 2004). Sampling took place a few days after the melting of snow on ice. On 14 March, ice surface was wet and slushy. The following cold and cloudless night resulted in freezing of the water and slush on the ice and increased the freeboard from 0 cm to +2 cm. Water in the study area had

a salinity of 5.3 at 2-m depth. Since surface melting had already started, salinity was 3.3 in the water right beneath the ice bottom.

Field sampling

Ice samples were collected using a 9-cm-diameter ice core drill on 14 March. The ice core was divided into three parts, surface (0–12 cm), middle (12–25 cm), and bottom (25–37 cm) ice layers, and analyzed for ice structure by thin sections (Weeks and Gow 1978), spectral absorption coefficient of CDOM (a_{CDOM}) and PM (a_p), chlorophyll *a* (Chl *a*) and MAA concentrations, and species composition of algae.

Optical measurements

Incident, reflected, and transmitted spectral irradiances were measured simultaneously with three Ramses-ACC VIS hyperspectral radiometers (TriOS Optical Sensors). These sensors measured upwelling or downwelling plane irradiances using cosine collector within wavelength range from 320 to 950 nm and sampling bandwidth of 3.3 nm. Measurements from two of the sensors were normalized to fit the measurements from the third sensor with cross-calibration of all sensors in the air. To measure transmitted irradiances, an aluminum arm with floats was used to position the sensors under the ice. The arm was installed through a 30 cm × 30 cm hole in the ice and the sensors were positioned 3 cm below the ice bottom, 1 m south of the hole. We also used a Macam SR991 spectroradiometer (Macam Photometrics) equipped with a cosine collector attached to a 4.2-m-long optical fiber to measure irradiances between 305 nm and 400 nm with a 2-nm bandwidth at 5-nm intervals. In this case, one single instrument was used to make successive measurements of incident, reflected, and transmitted irradiances. The replicated transmittance measurements ($n \geq 5$) with Macam had coefficient of variation of 8% and overlapped the measurements made simultaneously with the Ramses instruments. Irradiance measurements with Ramses instruments were expressed as the average of at least three scans, whereas for Macam measurements at least five scans were averaged. Measurements of upwelling and downwelling irradiance in the water column were conducted also with Ramses radiometers.

Irradiance attenuation in the interior of the ice was measured with an inverted Ramses radiometer following the method described by Grenfell et al. (2006). In this setup, the sensor was mounted on a 5-cm-diameter metal housing pointing downward to a diffuse reflector surface and then inserted into a 5.2-cm-diameter hole that was drilled through the ice and set to different depths at 5-cm intervals. The sensor head was also shaded, so that only radiation from the reflector surface entered the sensor.

Laboratory measurements

a_{CDOM} and a_p were measured from melted ice core samples (in dark +4°C overnight, no buffering with filtered seawater) that were filtered through glass fiber filters (Whatman GF/F 25-mm diameter, nominal pore size of 0.7 μm) in an all-glass filtration device (19-mm diameter of filtering area) with low vacuum. The filtrate was collected for a_{CDOM} measurements. The filters were placed into small dishes, kept in darkness, and a_p was measured within a few hours or from frozen (−18°C) filters on the next day. The CDOM spectra were measured against Milli-Q®-blanks from 200 nm to 800 nm with 2-nm slits and at 1-nm intervals using a Shimadzu UV-2501 PC spectrophotometer (Shimadzu). The absorbance measured with a 10-cm quartz cuvette (A_{CDOM}) was converted to an absorption coefficient ($a_{CDOM} = 2.303\ A_{CDOM}\ 0.1^{-1}$). In addition, spectral slope coefficients (S) were derived from CDOM absorption spectra by a linear fit to ln-transformed data:

$$a_{CDOM}(\lambda) = a_{CDOM}(\lambda_0)\, e^{-S(\lambda-\lambda_0)} \quad (1)$$

where λ_0 is a reference wavelength. In this study, three different wavelength ranges to determine S were used: 275–295 nm, 300–400 nm, and 350–400 nm. Also a dimensionless slope ratio S_R ($S_{275–295} : S_{350–400}$) was calculated (Helms et al. 2008). a_p was measured with an ISR-240A integrating sphere by the "transmittance–reflectance" method (Tassan and Ferrari 2002) using a quartz support, which allowed measurements also in the UV region. The optical density of particles on the filter was converted to an absorption coefficient by accounting for the path length amplification and the ratio of filtered volume to the filter area.

MAAs were extracted after 8 months of storage of filters at −19°C according to Tartarotti and Sommaruga (2002). Filters were placed in 5 mL of 20% methanol (v/v) and sonicated in ice with a VCX 600 sonicator (Sonics and Materials, power 600 W, frequency 20 kHz, for 1 min at 0.5 cycles and 20% amplitude). After 2 h of incubation at 45°C, the extract was filtered through 0.2-μm pore size membrane filters (Sartorius Minisart, syringe filter). The extraction was repeated, and the second extract was pooled with the first one. The extracts were freeze-dried, redissolved in 0.75 mL of 20% MeOH, placed in Eppendorf vials, and freeze-dried again. The dried extract was stored at −19°C before analysis.

MAAs were analyzed by high-performance liquid chromatography (Dionex) using a 250 mm × 4.6 mm Phenosphere 5-μm C8 column (Phenomenex) protected by a guard column (SecurityGuard, Phenomenex). The analysis was run on an isocratic reverse-phase mode with 0.1% acetic acid in 25% MeOH (v/v) as mobile phase. Absorbance was measured between 200 and 595 nm in 0.5-nm steps with a diode array detector (Dionex). During the analysis, the temperature in the autosampler and in the column was kept at 20°C and 15°C, respectively. Peaks were attributed to MAAs on the basis of their maximum absorption wavelength, spectrum, relative retention time, and cochromatography with pure standards. Peak area (acquired with the software Chromeleon, Dionex) was used to calculate MAAs concentrations as described in Tartarotti and Sommaruga (2006).

Samples for species identification were diluted with filtered seawater and kept in darkness at 1°C and processed directly after complete melting. Abundance of main algae groups were measured from 100-mL acid Lugol-fixed samples. Samples were settled in 50-mL (Ø 25 mm) chambers for approximately 15 h and inspected under an inverted light microscope. Samples for Chl *a* were filtered through 25-mm GF/F filters and the filters were immediately soaked in 96% ethanol and then extracted in an ultrasonic bath. The concentration of Chl *a* in the filtered ethanol extract was determined with a Shimadzu RF-5000 fluorometer (Shimadzu), using excitation at 450 nm and emission at 670 nm after calibration with Chl *a* standards (Vähätalo and Järvinen 2007).

Attenuation coefficients

Ice was assumed to be thick enough so that light attenuation could be calculated using an exponential decay function ($E_d[z] = E_d[z = 0]\, e^{-K_d z}$) (Maffione 1998; Maffione et al. 1998). Spectral diffuse attenuation coefficient for downwelling irradiance (K_d) for the whole ice cover was calculated from the measured downwelling incident irradiance at the surface ($E_d[z = 0_+]$) and the downwelling irradiance ($E_d[z]$) below the ice cover.

Ice interior K_d between 25 and 35 cm from the ice surface was determined at each wavelength using finite difference equation between two depths z_1 and z_2:

$$K_d(z) = \frac{-2}{[E_{d,ref1}(z_2) + E_{d,ref1}(z_1)]} \frac{E_{d,ref1}(z_2) - E_{d,ref1}(z_1)}{z_2 - z_1} \quad (2)$$

where $z = (z_1 + z_2)/2$ is the depth from the ice surface, $E_{d,refl}$ is the irradiance at given depth measured with a diffuse reflector. Grenfell et al. (2006) and Light et al. (2008) showed that the depth gradients of vertical irradiance profiles acquired in this manner are indistinguishable from those measured from undisturbed ice, when the measured irradiance field is diffuse. The ice cover was composed of two optically homogenous layers, a surface granular layer and a columnar ice layer below (6 and 31 cm thick, respectively), as determined from their crystal structure (Weeks and Gow 1978). The K_d for the granular layer was obtained by fitting the appropriate attenuation to match with the measured total ice K_d using the columnar ice K_d obtained with Eq. 2.

To relate inherent optical properties a (absorption coefficient) and b (scattering coefficient) to apparent optical property K_d a simple relation by Kirk (1991) was used

$$K_d = \sqrt{a^2 + Gab} \quad (3)$$

where coefficient G is dependent on the shape of the scattering phase function and varies between 0.233 and 0.264 (Kirk 1994). Maffione (1998) also found G to be a weak function of single-scattering albedo $\omega_0 = b/(a + b)$ and following this, G was set to 0.233 for granular ice and 0.245 for columnar ice layers in the visible wavelengths. Coefficient G in the UV range was acquired through iteration to fit the measured K_d with the calculated K_d and assuming that b in the UV range is the same as b in visible wavelengths, i.e., b is wavelength independent from 300 to 700 nm (Perovich 1993). In the PAR range b was calculated for each layer with Eq. 3 using the measured a and K_d. Maffione (1998) noted that Eq. 3 is valid only when the medium is highly scattering and single-scattering albedo $\omega_0 \geq 0.95$. Measurements had $\omega_0 = 0.989$ in the PAR range for the entire ice cover thickness. At UV wavelengths, ω_0 decreased with decreasing wavelength and approached the lower limit as a result of increased absorption at shorter wavelengths. At 305 nm ω_0 was 0.947, so Eq. 3 was also valid in the UV range.

Absorption coefficients

Total spectral absorption coefficient (a_{tot}) was calculated as the sum of all absorbing components in the ice and consisted of the measured a_{CDOM} and a_p and calculated absorption by pure ice and liquid brine (a_{i+b}). Absorption coefficient for pure ice was obtained from laboratory measurements by Grenfell and Perovich (1981) and Perovich and Govoni (1991). a_{i+b} was volume-weighted average of absorption for pure ice (95%) and absorption for clear ocean water (Smith and Baker 1981; Sogandares and Fry 1997) as brine (5%). The latter value (5%) was based on earlier measurements in the same area by Ehn et al. (2004). Our results were not sensitive to ice brine volume and even brine volume of 10% would have no observable influence on the results. No solid salts were expected to be present because the ice temperature was >−2°C.

Absorption by MAAs in ice was estimated as $a_{MAA} = a_p - a_{p,ref}$, where $a_{p,ref}$ is an estimate of a_p when MAAs were absent and was derived from a_p by assuming that the absorption spectrum is linear from 295 to 355 nm in the absence of MAAs. The chosen wavelength range was based on the change of shape of the a_p spectrum.

Radiative transfer model

The two-stream radiative transfer model described by Perovich (1990, 1993), with three ice layers (granular ice and two columnar ice layers), was used to calculate UVR and PAR exposure and UVR : PAR ratios in the ice. The same model was used to estimate the influence of snow cover, CDOM, and PM on the ratio and on the transmittance of the ice cover. In this study, UVR-to-PAR ratio was defined as the ratio of scalar quantum irradiance

at 325 nm to the integrated scalar quantum irradiance from 400 to 700 nm. Model was fitted with measured a_{CDOM} and a_p and calculated a_{i+b} to the measured albedo and transmittance by varying wavelength-independent b_{model}, which was different from b acquired with Eq. 3. The best fit was found by minimizing the mean square root error between measured and modeled values.

The model was used to study the effect of a_p, a_{CDOM}, ice, and snow on radiation conditions in ice, and transmittance through the whole snow and ice cover. Model cases were constructed to cover the large range of conditions encountered in the study area during an ice season. With these model runs it was possible to examine the importance of different factors on the light field in sea ice.

Six different model conditions were used to model UVR : PAR ratio and transmittance. In case 1, the model was run with the observed snow and ice conditions, a_p, and a_{CDOM}. Case 2 included the observed conditions plus 15 cm of wet snow cover on the ice. The absorption coefficient of snow was set to be equal to pure ice and scattering coefficient was set according to Perovich (1990). Model was thereafter run with otherwise observed conditions, but with altered CDOM absorption. In case 3, a_{CDOM} was set to 0. Case 4 represented ice immediately after freezing when the CDOM content in ice can be up to 53% of that in seawater (A. V. Vähätalo unpubl.), i.e., $a_{CDOM} = 0.53 \times a_{CDOM}$ (under-ice seawater). The a_{CDOM} of ice was in this case two times higher in the middle and bottom ice layers than the measured a_{CDOM} in the ice and five times higher in the surface ice layer. Case 5 represented otherwise the measured conditions except that $a_p = 0$. In case 6, a_{CDOM} and a_p were 0 to represent a situation where only ice and brine absorb radiation.

Results

CDOM absorption

In the studied coastal area of the Baltic Sea, PM and CDOM were the largest absorbing components in the ice cover at wavelengths < 600 nm (Fig. 1). Above 600 nm the absorption coefficient of ice and brine, a_{i+b}, was the largest. CDOM was the largest single absorber at wavelengths < 380 nm. When examining the distribution of a_{CDOM} throughout the ice column, the magnitude of a_{CDOM} was lower and spectrally different at the surface ice layer than at the layers below (Fig. 2a). For example, $a_{CDOM}(\lambda = 300\ nm)$ was 1 m^{-1} and 2.5 m^{-1} in the surface and middle layers, respectively. Surface-layer a_{CDOM} had also a distinctive shoulder from 320 to 380 nm, where a_{CDOM} did not follow the typical exponential form. The spectral slope coefficient, $S_{300–400}$, was lower in the surface layer than in the other layers (Table 1).

Absorption by PM

PM was the largest absorbing component over the whole ice thickness between 380 and 600 nm (Fig. 1) and had the characteristic Chl *a* absorption peak at 670 nm (Fig. 2b). In addition, a_p was the largest absorbing component in the surface layer and had a distinct peak between 320 and 345 nm, with the maximum of 0.73 m^{-1} found at 325 nm (Fig. 2b). This peak corresponded to the absorption peak by MAAs.

Scattering coefficient

On 14 March, scattering coefficient, b, was 13 m^{-1} in columnar ice and 430 m^{-1} in granular ice (Table 1). In the granular ice, b changed along with surface conditions and albedo (Fig. 3). With wet ice surface and freeboard 0 cm, b was 430 m^{-1} and increased to 800 m^{-1} on 15 March after the surface became dry and freeboard increased to +2 cm, resulting in the largest albedo and a highly scattering surface layer.

PAR and UVR attenuation in ice

The spectral diffuse attenuation coefficient for downwelling irradiance, K_d, was lowest at 565 nm in the surface layer, at 560 nm in the columnar layer, and at 575 nm in the under-ice water (Fig. 4). In the surface layer, freeboard and subsequent changes in b affected K_d. For example, $K_d(\lambda = 565\ nm)$ in the surface layer was 5.9 and 8.2 m^{-1} on 14 and 15 March, respectively, and $K_d(\lambda = 325\ nm)$ was 12.0 and 14.4 m^{-1}, respectively. Over the whole ice cover, $K_d(\lambda = 565\ nm)$ changed from 1.8 to 2.2 m^{-1} and $K_d(\lambda = 325\ nm)$ from 5.0 to 5.3 m^{-1} from 14 to 15 March. Surface conditions did not affect the K_d in columnar ice, which was 3.6 and 1.0 m^{-1} at 325 and 565 nm, respectively, on both days.

To asses the role of CDOM on the attenuation of PAR and UVR, we calculated K_d with Eq. 3 by setting $a_{CDOM} = 0$. These calculations indicated that CDOM contributed 42%, 36%, 33%, and 20% to attenuation in ice at 305 nm, 325 nm, 360 nm, and 550 nm, respectively. The importance of CDOM in attenuation increased with depth in the ice cover along with an increase in a_{CDOM} (Fig. 2a). In the surface layer, PM and especially MAAs contributed largely to the attenuation of UVR. For example $a_{CDOM}(\lambda = 325\ nm)$ contributed only 23% to attenuation in the surface layer compared with 45% in the columnar ice layer.

Transmittance

To extend our results over different optical conditions we modeled transmittances through whole ice cover (31-cm columnar and 6-cm granular ice) under six different conditions (Fig. 5). Model cases were (1) the measured conditions, (2) 15 cm of wet snow cover on ice, (3) no CDOM absorption ($a_{CDOM} = 0$), (4) high CDOM absorption ($a_{CDOM} = 0.53 \times a_{CDOM}$ [water]), (5) no PM absorption ($a_p = 0$), and (6) no CDOM or PM absorption ($a_{CDOM} = 0$ and $a_p = 0$). A comparison of cases 3 and 5 indicated that CDOM affected mostly the transmission of UVR, whereas PM had the largest influence on the transmission of PAR (Fig. 5). The wavelength of maximum transmittance shifted from 580 to 548 nm from high CDOM (case 4) to no CDOM (case 3), respectively. The measured wavelength of maximum transmittance, 562 nm (case 1), shifted to 492 nm in case 5 without PM. Without PM and CDOM (case 6), the wavelength of maximum transmittance shifted even further toward UVR. A snow layer on the ice (case 2) had a significant influence on transmittance, but high CDOM (case 4) had nearly the same influence on UVR transmittance. This emphasizes the importance of CDOM on UVR transmittance in young sea ice covers.

PAR and UVR in ice

At 12:00 h on 14 March, the downwelling plane quantum irradiance of PAR ($E_{d,PAR}$) was 709 and 351 μmol quanta m^{-2} s^{-1} above and under ice, respectively (Fig. 6). Modeled scalar quantum irradiances ($E_{o,q}$) inside the ice were larger than the measured $E_{d,q}$ as a result from scattering in the ice. For example, $E_{o,PAR}$ in the top of granular ice layer was 1.6 times larger than the measured $E_{d,PAR}$ above the ice (Fig. 6). The mean $E_{o,PAR}$ for the surface, middle, and bottom layers of ice were 629, 420, and 370 μmol quanta m_{-2} s_{-1}, respectively (Fig. 6). The $E_{o,PAR}$ below the ice exceeded the light-saturating irradiances (ca. 150 μmol quanta m^{-2} s^{-1}) for the dominant species of winter phytoplankton in our study region (Spilling 2007), indicating that the light intensities were high for the biological communities in and below the ice.

At 12:00 h on 14 March, the modeled mean $E_{o,q}(\lambda = 325\ nm)$ for surface, middle, and bottom layers were 0.31, 0.16, and 0.11 μmol quanta m^{-2} s^{-1}, respectively, and measured $E_{d,q}(\lambda = 325\ nm)$ under ice was 0.06 μmol quanta m^{-2} s^{-1}. The $E_{o,q}(\lambda = 305\ nm)$ was two orders of magnitude smaller than $E_{o,q}(\lambda = 325\ nm)$ (Fig. 6), which could account for the need of microalgae to produce photoprotective substances such as MAAs against UVR at

325 nm rather than protect themselves from potentially more damaging but much less intense shorter UVR.

UVR-to-PAR ratio

As the UVR at 325 nm was potentially the most damaging to organisms, we defined the UVR-to-PAR ratio, which describes the balance between potential for radiation-induced damage to potential for repair, as the ratio of radiation at 325 nm to the PAR. The UVR : PAR ratio was modeled under the six conditions that might be encountered during an ice season in the study area (Fig. 7). In all cases, except for those without CDOM (cases 3 and 6), there was a large difference in the UVR : PAR ratio between surface and bottom layers. The UVR : PAR ratios were smaller in the columnar ice layers at the bottom of the ice cover than in the surface layer (Fig. 7). These results (Fig. 7) indicate that CDOM was a very important factor in modifying UVR : PAR ratios and even more important than a 15-cm-thick overlying snow cover.

MAAs and the algae in the ice

MAAs were found in relatively high concentration in the ice (Table 1). The combined palythine and shinorine concentration was 1.37 μg L^{-1} (± 0.39 [SD]) in the surface layer and 0.39 μg L^{-1} (± 0.01) and 0.32 μg L^{-1} (± 0.21) in the middle and the bottom layers, respectively, resulting in MAA concentrations four times smaller in the bottom than in the surface. The MAAs-to-Chl *a* ratio was highest at the surface (0.65) and decreased toward the bottom (Table 1). In all layers, shinorine, with an absorption maximum at 334 nm, was more abundant than palythine, with an absorption maximum at 320 nm, and contributed 57%, 61%, and 65% of the total MAA concentration in surface, middle, and bottom layers, respectively.

MAAs contribution to the total absorption in the ice was significant: 10%, 3%, and 2% of $a_{tot}(\lambda = 325\ nm)$ in the surface, middle, and bottom ice layers, respectively. Thus MAAs contributed 14% to $a_p(\lambda = 325\ nm)$ over the whole ice cover thickness.

The algae in the ice consisted mostly of green algae (such as *Dictyosphaerium* sp.) in the granular layer and diatoms (*Nitschia frigida, Achnantes teniata, Amphiprora* sp., and *Chaetoceros* sp.) in the columnar ice layer, but dinoflagellates, predominately *Scrippsiella hangoei*, were found evenly distributed in all ice layers.

Discussion

The results presented in this study indicate that organic matter within sea ice can significantly modify UVR in and below the ice cover, especially when a snow cover is absent. CDOM, PM, and MAAs absorb significantly UVR in the ice and reduce the absolute UVR available and thus diminish the harmful biological effect of UVR in ice and under-ice water. In the surface layer, on the other hand, exposures to UVR can be enhanced by increased scalar irradiances due to high scattering in the ice.

MAAs in ice

MAAs are efficient in screening out UVR, apparently without producing damaging photoexcited states (Shick and Dunlap 2002) and there is supportive evidence for their direct photoprotective role in primary producers (reviewed in Banaszak 2003). The primary producers we found in the ice cover included diatoms and dinoflagellates, which are known to produce MAAs (Jeffrey et al. 1999). In our study, MAA concentrations were high and similar to those found for surface phytoplankton in lakes transparent to UVR (Sommaruga and Garcia-Pichel 1999). The high MAA concentrations in our study are probably a

consequence of the high UVR exposure and UVR : PAR ratio in the ice surface. In the surface layer, where the CDOM absorption was low, but scalar irradiances were high due to scattering, MAAs seem to be crucial in attenuating UVR.

The only published study about MAAs in sea ice reported MAAs-to-Chl *a* ratios < 0.02 for the bottom of the ice, which are much lower than our highest ratio of 0.65 (Ryan et al. 2002). The high ratio of MAAs to Chl *a* in our study was not related to low Chl *a* values, because our Chl *a* concentrations in the ice were similar or slightly lower than values reported earlier for Baltic Sea ice (Ehn et al. 2004; Kuparinen et al. 2007). Ryan et al. (2002) concluded that MAAs had a minor role as photoprotectants in sea ice algae in the area they studied. They studied, however, only the bottom-ice algal community under initially snow-covered ice where MAAs are expected to have low concentrations. Our study indicates that MAAs contribute significantly to ice optical properties, especially in the surface layer, where $a_{CDOM,UVR}$ is low and $E_{o,UVR}$ is high because of strong scattering in the surface layer. In our study site, the biosynthesis of MAAs may also benefit from the high concentration of nitrogen (up to 2.3 μmol L^{-1}) in the Baltic Sea ice (Litchman et al. 2002; Kaartokallio et al. 2007). In our study, there was also a strong relation between MAA concentration, UVR intensity, and UVR : PAR ratio (R^2 = 0.97, n = 3).

Belzile et al. (2000) suspected the presence of MAAs in the Arctic sea ice. However, they based their assumption solely on a distinct shoulder (320–380 nm) in the CDOM absorption spectra that could be associated with MAAs. A similar shoulder was also observed in the surface layer in our measurements (Fig. 2a).

Transmittance and attenuation in ice

The shape and magnitude of K_d for the whole ice cover in our study were very similar to those reported by Ehn et al. (2004) for the Baltic Sea. Our K_d at wavelengths > 550 nm in columnar layer were also similar to values reported for Arctic first-year ice interior (Light et al. 2008), and whole ice-cover K_d was very similar to Arctic “dirty” multiyear ice (Pegau and Zaneveld 2000; Light et al. 2008). Ice cover is typically thinner in the Baltic Sea than in the Arctic and with similar K_d in the ice cover, the PAR transmittances are typically two to four times lower in the Arctic than in our study (Perovich et al. 1998; Belzile et al. 2000).

Our K_d values at wavelengths < 550 nm differ from those reported from the Arctic (Pegau and Zaneveld 2000; Light et al. 2008). In Arctic sea ice, K_d between 400 and 550 nm is spectrally flat, in contrast to our study where K_d increased with decreasing wavelength as a result of significant CDOM and PM absorption. Despite the large differences in ice thickness, the in-ice and under-ice UVR intensities are typically very similar between the Baltic Sea and the Arctic, as a consequence of the difference in K_d (Perovich et al. 1998; Perovich 2006). The thickness and properties of the surface scattering layer largely affect both UVR and PAR transmittances through the ice cover.

In the Arctic, the wavelength of maximum transmittance of sea ice ranges between 460 and 570 nm depending on the concentration of PM, which shifts the maximum toward longer wavelengths (Perovich et al. 1993; Perovich et al. 1998; Light et al. 2008). This shift agrees well with our modeled transmittances with different concentrations of dissolved and particulate inclusions in ice (Fig. 5). The wavelength of maximum transmittance at around 570 nm in the Arctic sea ice (Perovich et al. 1993, 1998; Light et al. 2008) suggests that in some cases, Arctic sea ice can contain similar concentrations of PM as found in our study.

Absorption and scattering in ice

In the columnar ice, a_{CDOM} values found in this study were similar to those from other studies made in the Baltic Sea area (Ehn et al. 2004; Stedmon et al. 2007). Our low a_{CDOM}

at the surface layer could be a combined result from CDOM deposited from the atmosphere and the photochemical alteration of CDOM (Kieber et al. 2007). However, the a_{CDOM} of melting ice can be higher at the surface than in the ice layers below (Ehn et al. 2004). The high a_{CDOM} of surface ice can be a result of flooding of the ice cover with seawater during snow–ice formation, which can introduce "fresh" CDOM to the ice surface (Granskog et al. 2004). The values of a_{CDOM} reported from other sea ice regimes are sparse and the only comparable results are those reported by Belzile et al. (2000) for the Canadian Arctic. Their a_{CDOM} are similar in magnitude to those found in our study, with most $a_{CDOM}(\lambda = 300\ nm)$ values found between 0.4 and 2 m^{-1}, and are also lower in the surface ice layers. This is an intriguing similarity because dissolved organic carbon concentrations are three to four times higher in the Baltic Sea water (Hagström et al. 2001) than in that area. The S-values found in the present study were in agreement with other studies in the Baltic Sea (Ehn et al. 2004) and S_R values (Table 1) corresponded to values reported by Helms et al. (2008) for a coastal river–ocean mixed water. The potential contribution of lysing cells to a_{CDOM} measurements was considered negligible as all the major pigments and the most absorbing PM are poorly soluble to water after depigmentation with NaClO bleaching (Seppälä et al. 2005). The water-soluble lysate of algae is poorly pigmented at the visible range of spectrum but the water-soluble MAAs may contribute to CDOM and this is the most likely explanation to a distinct shoulder (320–380 nm) in the CDOM absorption spectra observed in the surface layer in our measurements (Fig. 2a).

Our $a_{p,PAR}$ was also similar to that reported earlier in the same region (Ehn et al. 2004) and on average two to three times higher for the entire ice thickness than results reported for the Arctic sea ice on average (Perovich et al. 1998; Belzile et al. 2000). Nevertheless, $a_{p,PAR}$ can be approximately the same in highly absorbing surface and bottom layers of Arctic first-year sea ice than found in our study (Perovich et al. 1998; Belzile et al. 2000). To our knowledge, our results are the first reported sea ice a_p measurements in the UVR, and show that a_p can be larger in the UVR than in the PAR region (Fig. 2). Thus, a_p can be an important factor contributing to sea ice optical properties at UV wavelengths and also point toward the presence of MAAs in the ice.

The b obtained in this study agree well with the results from Arctic first-year ice by Light et al. (2008), where they reported b between 350 and 1100 m^{-1} for the surface layer depending on the surface conditions and between 8 and 30 m^{-1} for the interior of ice. This similarity indicates that scattering properties for level sea ice (without melt ponds) are governed by ice type rather than location.

Implications of the UVR-to-PAR ratio for ice communities

The potential effect of UVR : PAR ratio on the biology is evident from our results when comparing MAA concentrations in the surface and middle layers. There were larger differences in MAA concentrations (Table 1) than in $E_{o,q}(\lambda = 325\ nm)$ between the surface and middle layers (Fig. 6). Our optical model showed that $E_{o,q}(\lambda = 325\ nm)$ was 2.3 times higher in the surface layer than in the middle layer (Fig. 6), but MAA concentration was 3.5 times higher in the surface layer. As mentioned above, large UVR : PAR ratio could explain the high concentration of MAAs in relation to UVR at the surface (Table 1).

The UVR : PAR ratios in the model case without CDOM (case 3) were comparable with the ratios reported by Perovich (1993) for Antarctic sea ice. In the presence of CDOM, our ratios were smaller than the ones reported by Perovich (1993). This indicates that CDOM absorbs UVR effectively in the ice and strongly modifies the UVR : PAR ratio, as the ratio at the ice bottom would have been almost two times larger without CDOM (Fig. 7).

When comparing the optical properties of ice between our study and the Arctic, the high UVR : PAR ratio in Arctic ice makes biological communities potentially susceptible to UVR. During spring and summer in the Arctic, high UVR intensities and UVR : PAR ratios are expected in the ice because of typically low UVR attenuation and high incident UVR (Perovich et al. 1998; Belzile et al. 2000; Perovich 2006).

Acknowledgments

We thank H. Kuosa, E. Eronen, and D. Nomura for the data on algae species composition and chlorophyll *a*.

This work was supported by grants from Walter and Andrée de Nottbeck Foundation, Academy of Finland (108150) to M.A.G., and the Austrian Science Fund (FWF, P19245) to R.S.

References

Arrigo, KR. Primary production in sea ice, p. 143–183. In: Thomas, DN.; Dieckmann, GS., editors. Sea ice: An introduction to its physics, chemistry, biology and geology. Blackwell Science; 2003.

Banaszak, AT. Photoprotective physiological and biochemical responses of aquatic organisms, p. 329–358. In: Helbling, EW.; Zagarese, H., editors. UV effects in aquatic organisms and ecosystems. Comprehensive Series in Photochemical and Photobiological Sciences. Royal Society of Chemistry; 2003.

Belzile C, Johannessen SC, Gosselin M, Demers S, Miller WL. Ultraviolet attenuation by dissolved and particulate constituents of first-year ice during late spring in an Arctic polynya. Limnol. Oceanogr. 2000; 45:1265–1273.

Cota GF, Legendre L, Gosselin M, Ingram RG. Ecology of bottom ice algae: I. Environmental controls and variability. J. Mar. Syst. 1991; 2:257–277.

Ehn J, Granskog MA, Reinart A, Erm A. Optical properties of melting landfast sea ice and underlying seawater in Santala Bay, Gulf of Finland. J. Geophys. Res. 2004; 109:C09003. doi: 10.1029/2003JC002042.

Granskog MA, Leppäranta M, Kawamura T, Ehn J, Shirasawa K. Seasonal development of the properties and composition of landfast sea ice in the Gulf of Finland, the Baltic Sea. J. Geophys. Res. 2004; 109:C02020. doi:10.1029/2003JC001874.

Grenfell TC, Light B, Perovich DK. Spectral transmission and implications for the partitioning of short-wave radiation in arctic sea ice. Ann. Glaciol. 2006; 44:1–6. doi: 10.3189/172756406781811763.

— , Perovich DK. Radiation absorption-coefficients of polycrystalline ice from 400–1400 nm. J. Geophys. Res. 1981; 86:7447–7450.

Hagström Å, Azam F, Kuparinen J, Zweifel UL. Pelagic plankton growth and resource limitations in the Baltic Sea. Syst. Anal. Balt. Sea. 2001; 148:177–210.

Helms JR, Stubbins S, Ritchie JD, Minor EC, Kieber DJ, Mopper K. Absorption spectral slopes and slope ratios as indicators of molecular weight, source, and photobleaching of chromophoric dissolved organic matter. Limnol. Oceanogr. 2008; 53:955–969.

Jeffrey SW, Mactavish HS, Dunlap WC, Vesk M, Groenewoud K. Occurrence of UVA- and UVB-absorbing compounds in 152 species (206 strains) of marine microalgae. Mar. Ecol. Prog. Ser. 1999; 189:35–51.

Kaartokallio H, Kuosa H, Thomas DN, Granskog MA, Kivi K. Biomass, composition and activity of organism assemblages along a salinity gradient in sea ice subjected to river discharge in the Baltic Sea. Polar Biol. 2007; 30:183–197.

Kawamura T. Time-series observations of the structure and properties of brackish ice in the Gulf of Finland. Ann. Glaciol. 2001; 33:1–4. OTHERS.

Kieber RJ, Willey JD, Whitehead RF, Reid SN. Photobleaching of chromophoric dissolved organic matter (CDOM) in rainwater. J. Atmos. Chem. 2007; 58:219–235.

Kirk JTO. Volume scattering function, average cosines, and the underwater light-field. Limnol. Oceanogr. 1991; 36:455–467.

— . Characteristics of the light-field in highly turbid waters: a Monte-Carlo study. Limnol. Oceanogr. 1994; 39:702–706.

Kuparinen J. Role of sea-ice biota in nutrient and organic material cycles in the northern Baltic Sea. Ambio. 2007; 36:149–154. OTHERS. [PubMed: 17520927]

Laurion I, Ventura M, Catalan J, Psenner R, Sommaruga R. Attenuation of ultraviolet radiation in mountain lakes: Factors controlling the among- and within-lake variability. Limnol. Oceanogr. 2000; 45:1274–1288.

Light B, Grenfell TC, Perovich DK. Transmission and absorption of solar radiation by Arctic sea ice during the melt season. J. Geophys. Res. 2008; 113:C03023. doi:10.1029/2006JC003977.

Litchman E, Neale PJ, Banaszak AT. Increased sensitivity to ultraviolet radiation in nitrogen-limited dinoflagellates: Photoprotection and repair. Limnol. Oceanogr. 2002; 47:86–94.

Maffione RA. Theoretical developments on the optical properties of highly turbid waters and sea ice. Limnol. Oceanogr. 1998; 43:29–33.

— , Voss JM, Mobley CD. Theory and measurements of the complete beam spread function of sea ice. Limnol. Oceanogr. 1998; 43:34–43.

Palosuo E. Crystal structure of brackish and fresh-water ice. Int. Assoc. Sci. Hydrol. 1961; 54:9–14.

Pegau WS, Zaneveld JRV. Field measurements of in-ice radiance. Cold Reg. Sci. Technol. 2000; 31:33–46.

Perovich DK. Theoretical estimates of light-reflection and transmission by spatially complex and temporally varying sea ice covers. J. Geophys. Res. 1990; 95:9557–9567.

— . A theoretical-model of ultraviolet-light transmission through Antarctic sea-ice. J. Geophys. Res. 1993; 98:22579–22587.

— . Complex yet translucent: The optical properties of sea ice. Physica B. 2003; 338:107–114.

— . The interaction of ultraviolet light with Arctic sea ice during SHEBA. Ann. Glaciol. 2006; 44:47–52. doi:10.3189/172756406781811330.

— , Cota GF, Maykut GA, Grenfell TC. Bio-optical observations of first-year Arctic sea-ice. Geophys. Res. Lett. 1993; 20:1059–1062.

— , Govoni JW. Absorption-coefficients of ice from 250 to 400 nm. Geophys. Res. Lett. 1991; 18:1233–1235.

— , Roesler CS, Pegau WS. Variability in Arctic sea ice optical properties. J. Geophys. Res. 1998; 103:1193–1208.

Prezelin, BB.; Moline, MA.; Matlick, HA. Icecolors ’93: Spectral UV radiation effects on Antarctic frazil ice algae, p. 45–83. In: Lizotte, M.; Arrigo, K., editors. Antarctic sea ice: Biological process, interactions, and variability. AGU; 1998. Antarctic Research Series

Ryan KG, McMinn A, Mitchell KA, Trenerry L. Mycosporine-like amino acids in antarctic sea ice algae, and their response to UVB radiation. Z. Naturforsch. 2002; 57:471–477.

Seppälä J, Ylöstalo P, Kuosa H. Spectral absorption and fluorescence characteristics of phytoplankton in different size fractions across a salinity gradient in the Baltic Sea. Int. J. Remote Sens. 2005; 26:387–414.

Shick JM, Dunlap WC. Mycosporine-like amino acids and related gadusols: Biosynthesis, accumulation, and UV-protective functions in aquatic organisms. Annu. Rev. Physiol. 2002; 64:223–262. [PubMed: 11826269]

Smith RC, Baker KS. Optical properties of the clearest natural waters (200–800 nm). Appl. Opt. 1981; 20:177–184. [PubMed: 20309088]

Sogandares FM, Fry ES. Absorption spectrum (340–640 nm) of pure water. I. Photothermal measurements. Appl. Opt. 1997; 36:8699–8709. [PubMed: 18264419]

Sommaruga R, Garcia-Pichel F. UV-absorbing mycosporine-like compounds in planktonic and benthic organisms from a high-mountain lake. Arch. Hydrobiol. 1999; 144:255–269.

— , Psenner R. Ultraviolet radiation in a high mountain lake of the Austrian Alps: Air and underwater measurements. Photochem. Photobiol. 1997; 65:957–963.

Spilling K. Dense sub-ice bloom of dinoflagellates in the Baltic Sea, potentially limited by high pH. J. Plankton Res. 2007; 29:895–901.

Stedmon CA, Thomas DN, Granskog M, Kaartokallio H, Papadimitriou S, Kuosa H. Characteristics of dissolved organic matter in Baltic coastal sea ice: Allochthonous or autochthonous origins? Environ. Sci. Technol. 2007; 41:7273–7279. [PubMed: 18044499]

Tartarotti B, Sommaruga R. The effect of different methanol concentrations and temperatures on the extraction of mycosporine-like amino acids (MAAs) in algae and zooplankton. Arch. Hydrobiol. 2002; 154:691–703.

— , — . Seasonal and ontogenetic changes of mycosporine-like amino acids in planktonic organisms from an alpine lake. Limnol. Oceanogr. 2006; 51:1530–1541. [PubMed: 21258624]

Tassan S, Ferrari GM. A sensitivity analysis of the 'Transmittance–Reflectance' method for measuring light absorption by aquatic particles. J. Plankton Res. 2002; 24:757–774.

Thomas, DN.; Papadimitriou, S. Biogeochemistry of sea ice, p. 267–302. In: Thomas, DN.; Dieckmann, GS., editors. Sea ice: An introduction to its physics, chemistry, biology and geology. Blackwell Science; 2003.

Vähätalo AV, Järvinen M. Photochemically produced bioavailable nitrogen from biologically recalcitrant dissolved organic matter stimulates production of a nitrogen-limited microbial food web in the Baltic Sea. Limnol. Oceanogr. 2007; 52:132–143.

Weeks WF, Gow AJ. Preferred crystal orientations in the fast ice along the margins of the Arctic Ocean. J. Geophys. Res. 1978; 83:5105–5121.

Europe PMC Funders Author Manuscripts

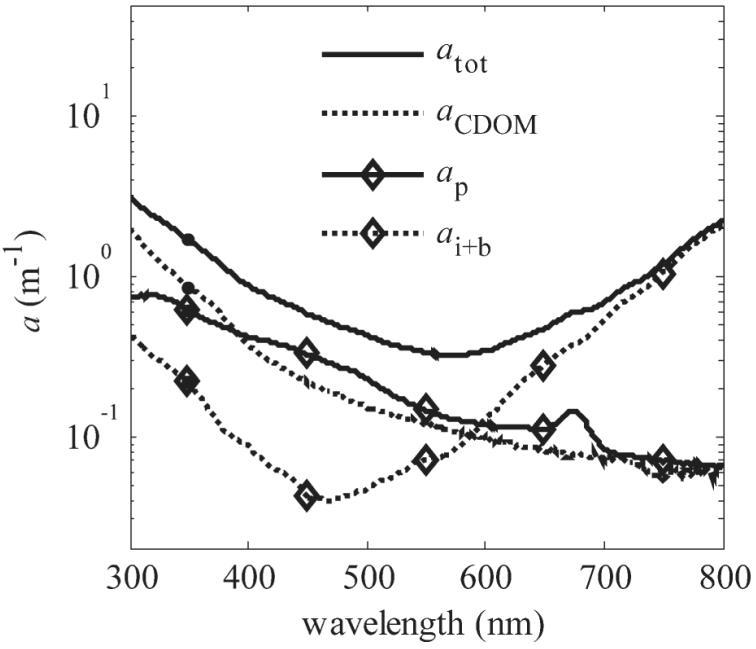

Fig. 1.

Mean spectral absorption coefficients for total absorption (a_{tot}), colored dissolved organic matter (a_{CDOM}), particulate matter (a_p), and ice and brine combined (a_{i+b}) (Grenfell and Perovich 1981; Smith and Baker 1981; Perovich and Govoni 1991; Sogandares and Fry 1997) over the whole ice thickness on 14 March 2007.

Europe PMC Funders Author Manuscripts

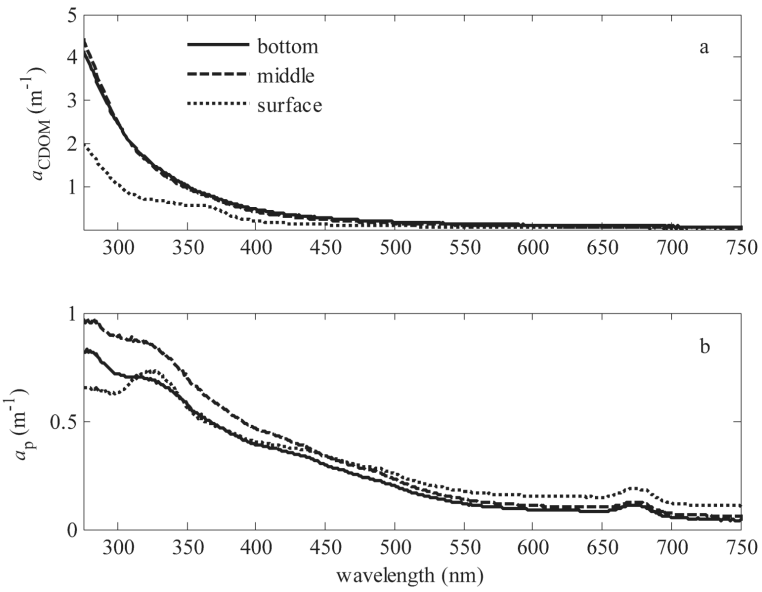

Fig. 2.
(a) a_{CDOM} and (b) a_p for three ice layers: surface 0–12 cm, middle 12–25 cm, and bottom 25–37 cm on 14 March 2007.

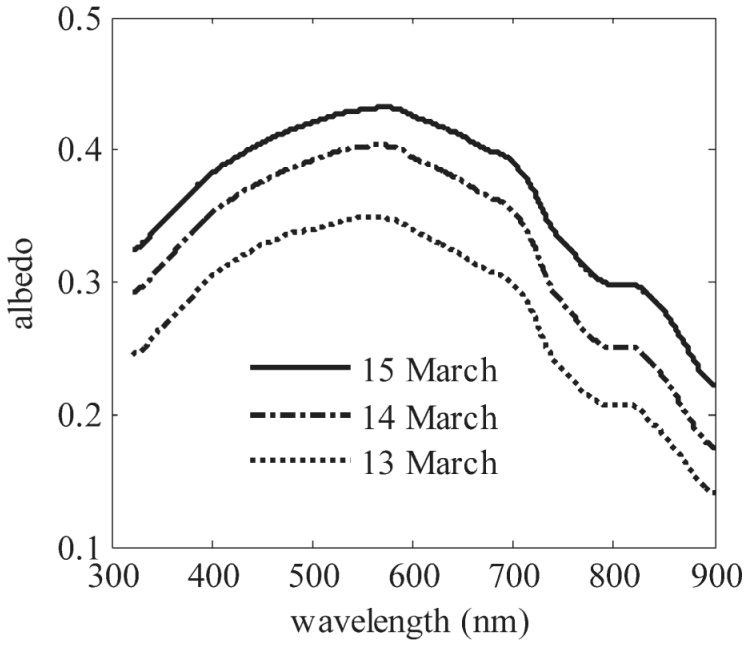

Fig. 3.
Spectral albedo during three consecutive days in March 2007. Surface was wet and freeboard 0 cm on 13 March and then surface dried out and freeboard increased to +2 cm on 15 March.

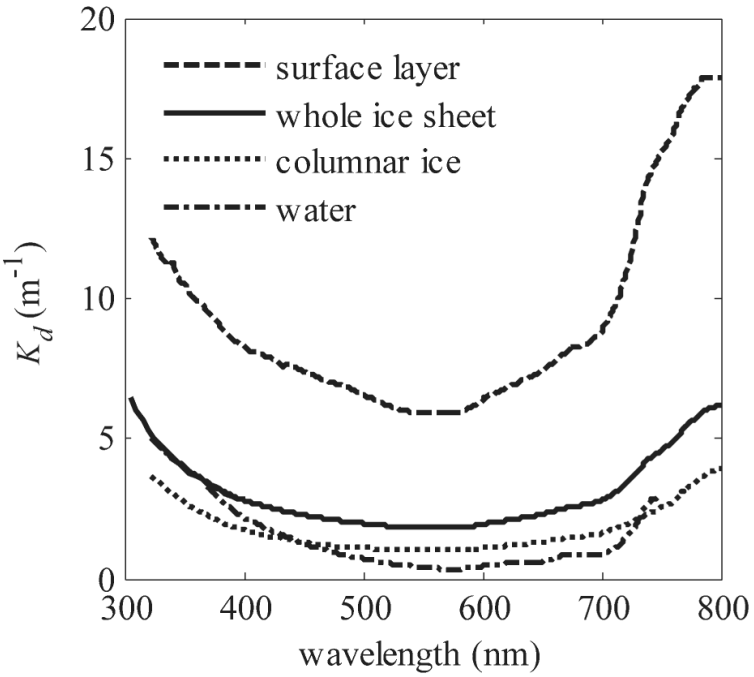

Fig. 4.

Calculated (surface layer) and measured (whole ice sheet, columnar ice, and water 20–70 cm below ice bottom, on 14 March) K_d. Entire ice thickness K_d shows the overlapping results from measurements with two different instruments (Ramses, 322–800 nm, and Macam, 305–400 nm, spectroradiometers; *see* text for details).

Europe PMC Funders Author Manuscripts

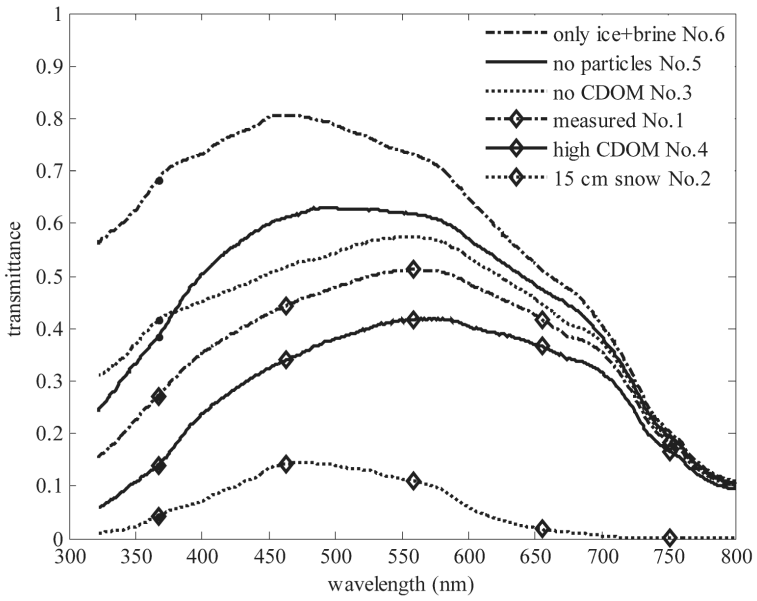

Fig. 5.

Measured and modeled transmittances for whole ice thickness (37-cm thick with 6-cm granular ice layer) with different PM and CDOM concentrations in ice and with 15 cm of wet snow layer on top of ice.

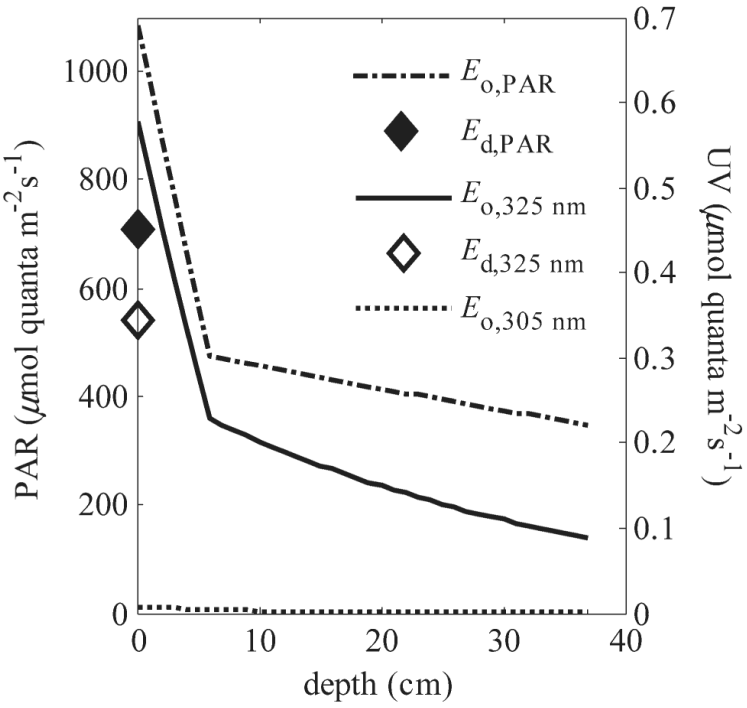

Fig. 6.

Measured downwelling plane quantum irradiance ($E_{d,q}$) for PAR and 325-nm radiation at the ice surface and modeled scalar quantum irradiance ($E_{o,q}$) at different depths in the ice cover on 14 March. The ice surface is indicated as 0 cm, whereas 6 cm is the bottom of granular ice layer, and 37 cm the bottom of ice. Model was run with the measured ice properties (case 1). PAR scale is on the left side and 305- and 325-nm scale on the right side *y*-axis.

Europe PMC Funders Author Manuscripts

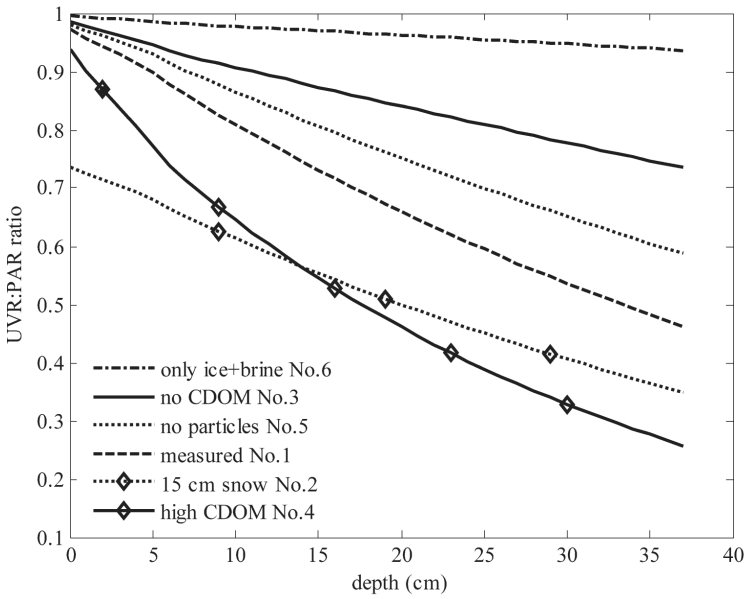

Fig. 7.

Modeled UV : PAR irradiance ratios in the ice cover at different depths for various PM, CDOM, and ice conditions (same as in Fig. 5). Ratio is normalized to incident irradiance ratio at the air–snow (when snow present) or air–ice surface (when no snow); depth 0 cm corresponds to ice top surface (ratios inside snow cover are not shown).

Europe PMC Funders Author Manuscripts

Table 1

Optical properties and the concentrations of Chl *a*, shinorine, and palythine of the three ice layers on 14 March 2007. UVR:PAR ratio is normalized to incident radiation ratio right above the ice surface. Ice layers are surface 0–12-cm, middle 12–25-cm, and bottom 25–37-cm depth from ice surface.

	b (m^{-1})	$S_{300–400}$ (nm^{-1})	S_R	Chl *a* ($\mu g\ L^{-1}$)	Shinorine (SD) ($\mu g\ L^{-1}$)	Palythine (SD) ($\mu g\ L^{-1}$)	UVR: PAR
Surface	430 *	0.013	1.12	2.1 *	0.78(0.22)	0.59(0.17)	0.88
Middle	13	0.017	1.35	1.5	0.24(0.01)	0.15(0.01)	0.68
Bottom	13	0.016	1.39	6.5 †	0.21(0.13)	0.11(0.07)	0.53

*Granular layer (top 6 cm of ice).

†Bottom 2 cm of ice.